AIP Journal of Applied Physics

The influence of Mn substitution on the local structure of Na0.5Bi0.5TiO3 crystals: Increased ferroelectric ordering and coexisting octahedral tilts

Jianjun Yao, Wenwei Ge, Li Yan, William T. Reynolds, Jiefang Li, D. Viehland, D. A. Kiselev, A. L. Kholkin, Qinhui Zhang, and Haosu Luo

Citation: Journal of Applied Physics **111**, 064109 (2012); doi: 10.1063/1.3699010
View online: http://dx.doi.org/10.1063/1.3699010
View Table of Contents: http://scitation.aip.org/content/aip/journal/jap/111/6?ver=pdfcov
Published by the AIP Publishing

The influence of Mn substitution on the local structure of $Na_{0.5}Bi_{0.5}TiO_3$ crystals: Increased ferroelectric ordering and coexisting octahedral tilts

Jianjun Yao,[1,a)] Wenwei Ge,[1] Li Yan,[1] William T. Reynolds,[1] Jiefang Li,[1] D. Viehland,[1] D. A. Kiselev,[2] A. L. Kholkin,[3] Qinhui Zhang,[4] and Haosu Luo[4]
[1]*Department of Materials Science and Engineering, Virginia Tech, Blacksburg, Virginia 24061, USA*
[2]*National University of Science and Technology "MISiS", Leninsky prospect 4, Moscow 119049, Russia*
[3]*Department of Ceramics and Glass Engineering, CICECO, University of Aveiro, Aveiro 3810–193, Portugal*
[4]*Shanghai Institute of Ceramics, Chinese Academy of Sciences, 215 Chengbei Road, Jiading, Shanghai 201800, China*

(Received 14 November 2011; accepted 25 February 2012; published online 29 March 2012)

The ferroelectric domain structure of pure $Na_{1/2}Bi_{1/2}TiO_3$ (NBT) and 1 at.% Mn-doped NBT (Mn-NBT) crystals was investigated by piezoresponse force microscopy. The correlation length of the polar regions was found to increase upon Mn substitution. High resolution transmission electron microscopy revealed that the coherency of the lattice across the domain boundaries between polar regions was also enhanced. Selected area electron diffraction showed that Mn favored coexisting 1/2 (ooo) and 1/2 (ooe) oxygen octahedral tiltings, over only 1/2 (ooo) for pure NBT. © *2012 American Institute of Physics*. [http://dx.doi.org/10.1063/1.3699010]

INTRODUCTION

Piezoelectric materials are commercially used in many applications, such as actuators, sensors, and transducers. For a long time, the dominant material used in these electromechanical devices has been Pb-based perovskites, such as $Pb(Zr_{1-x}Ti_x)O_3$ (PZT).[1] Environmental concerns are driving the need to replace Pb-based piezoelectrics. In 2004, the finding of high electrically induced strains in the Pb-free piezoelectric ceramic solid solution $(K,Na)NbO_3$ (KNN) triggered significant efforts directed at the elimination of Pb in piezoelectric perovskites.[2] Furthermore, recent investigations of $Na_{1/2}Bi_{1/2}TiO_3$-xat.%$BaTiO_3$(NBT-x%BT) have revealed giant strain and longitudinal piezoelectric constants as high as $d_{33} = 500$ pC/N for compositions near a morphotropic phase boundary (MPB) around $x = 5.5–6.5$.[3–13]

In spite of a non-rhombohedral average structure model for NBT at room temperature was supported by high-resolution single-crystal x ray diffraction,[14] it is still widely accepted that NBT undergoes a phase transformational sequence of paraelectric cubic (C) → paraelectric tetragonal (T) → ferroelectric rhombohedral (R) on cooling,[15–22] with transition temperatures of about 550 and 300 °C, respectively. It has been proposed that NBT has an intermediate orthorhombic bridging phase between T and R ones.[23,24] Recent temperature-dependent domain studies of NBT crystals by polarized light microscopy (PLM) have shown that T ferroelastic domains persist on cooling into the R phase field. Piezoresponse force microscopy (PFM) has revealed that ferroelectric R nanodomains nucleate within the geometrical restrictions of the T ferroelastic domains.[22] Support of these observations has also been reported by anelastic measurements.[6] High resolution transmission electron microscopy (HRTEM) has shown that the lattice is partially incoherent across the boundaries between polar nano-regions.[25] Formation of planar defects along the domain boundaries may help relax the elastic energy in this geometrically frustrated condition. Recent Raman studies of NBT have revealed no evidence of a structural phase transition near $T = 370$ K for $x > 0.055$, where dielectric anomalies have shown a transition.[26] Mixed rhombohedral (R3c) and tetragonal (P4bm) phases have been reported near the MPB by transmission electron microscopy (TEM).[27]

The mechanism of enhanced piezoelectricity near the MPB of NBT-x%BT is still an open question. Monoclinic (M) bridging phases have not yet been reported near the MPB, which are the origins of high piezoelectricity in $Pb(Mg_{1/3}Nb_{2/3})O_3$-xat%$PbTiO_3$ (PMN-x%PT) and $Pb(Zn_{1/3}Nb_{2/3})O_3$-xat%$PbTiO_3$ (PZN-%PT) crystals.[28–35] It has been reported that Mn substitution in NBT-x%BT crystals for compositions near the MPB can effectively increase the value of d_{33} from 280 to 480 pC/N.[4] This could be due to a more complete poling enabled by enhanced resistivity[4] and also, in part, from changes in the phase stability or domain structure.[5] Doping is known to modify the crystal structure and improve material properties: examples include La and K in PZT,[36–39] Sr and Ta in $NaNbO_3$,[40–43] and Ca and Sm in $BiFeO_3$.[44–48] Crystals of Mn-doped NBT have been reported to have: (i) enhanced resistivities, remnant polarizations, coercive fields, and d_{33} values; (ii) a slight decrease in the phase transformation temperatures; and (iii) a decrease in the size of the T ferroelastic domains.[49] It is noted that the addition of Mn has little effect on the properties of NBT ceramics at room temperature,[50] which might indicate subtle differences between crystals and ceramics, possibly due to changes in stress accommodation of domains. High-resolution synchrotron x ray diffraction (XRD) of both NBT and Mn-NBT have shown a broad transition range characterized by T and R phase coexistence on heating; no distinct difference has been found.[51]

The evolution of the domain and local structure for NBT with Mn substitution has not yet been reported. Domains

a)Electronic mail: jjyao@vt.edu.

make an important contribution to the dielectric and piezoelectric properties of ferroelectric materials. PFM is a powerful technique by which to study ferroelectric domains. It is based on the detection of local vibrations of a ferroelectric sample induced by a testing ac signal applied between a conductive tip and a bottom electrode. Oscillations of the sample underneath the tip modulate the deflection signal. The phase and amplitude of the oscillations, as measured by a lock-in method, depend on the orientation of the polarization. As a result, different domain variants can be distinguished by variations in the contrast of PFM images.[52] Because of these advantages, PFM has been used to map the domain distributions of many ferroelectrics.[52–55]

Here, we have used PFM to map the ferroelectric domain structures for Mn-NBT and have compared the images to those obtained for NBT. The images evidence an increased ordering of polar nano-regions by Mn. Lattice images reveal that modest additions of Mn effectively decrease the number of planar defects at the boundaries between polar regions, while favoring coexisting in-phase and anti-phase octahedral tiltings.

EXPERIMENTAL SECTION

Single crystals of NBT and Mn-NBT were grown by a top-seeded solution growth (TSSG) method at the Shanghai Institute of Ceramics. Starting materials of Na_2CO_3, Bi_2O_3, TiO_2, and $BaCO_3$ with purities of >99.99% were used, which were weighed according to their molar ratios. After these compounds were ground and mixed, they were put into a platinum (Pt) crucible and heated to 1200 °C for 10 h to decompose the carbonates and to form NBT polycrystals. The NBT polycrystals were ground and mixed with a 20% weight excess of Na_2CO_3 and Bi_2O_3 added as a self-flux for compensating compositional changes during single crystal growth. Single crystals were then grown from a Pt crucible, which was heated using a resistance furnace in an air atmosphere. A platinum wire was used as a seed for crystal growth. In order to avoid polycrystal formation during crystal growth, a temperature of 30–50 °C higher than the melting point was initially used. This was done to melt the microcrystal particles: such a condition was maintained for one hour. The growth temperature was then lowered to the melting temperature. Initially, single crystal formation was obtained by spontaneous nucleation at the end of the platinum wire, restricting the diameter of the crystalline material. The pulling rate was 2–2.5 mm per day after the crystal diameter reached a particular value, and the rotation rate was 10–30 rpm. After growth, the crystal was cooled to room temperature at a rate of 30–50 °C/h.

For the Mn-doped NBT crystals, 1 at.% MnO_2 was added in the precursors. The actual concentration of Mn in the as-grown Mn-NBT crystals was experimentally determined by x ray fluorescence (XRF) analysis. ⟨001⟩ oriented wafers of NBT and Mn-NBT single crystals were cut into dimensions of $3 \times 3 \times 0.5$ mm^3, and the surfaces were polished to a 50-nm finish. Samples were poled under 3–5 kV/mm for 15 min at 120 °C in silicon oil.

Investigations of the domain structure were performed by scanning probe microscopy using a piezoresponse force mode (Veeco Multi Mode DI 3100a with Nanoscope V controller). Gold electrodes were deposited on the bottom face of each crystal by sputtering. During the PFM studies, the electrode faces were glued to the sample stage and the opposite unelectroded surface was scanned by the SPM tip. All scans were performed at room temperature, using a conductive silicon tip coated with cobalt. An ac modulation voltage of 5 V_{pp} (peak to peak) with a frequency of 20 kHz was applied between the conductive tip and the bottom gold electrode.

Samples for TEM were prepared by mechanical polishing, followed by a dimple grinder thinning process, and finally followed by argon ion thinning at 4 kV to electron transparency. The specimens were taken to a final polish under 2 kV for 20 min to remove surface artifacts before TEM examination. Selected area electron diffraction (SAED) and bright field image studies were performed using a Philips EM 420 electron microscopy working at 120 kV equipped with a double-tilt sample holder to enable access to various zone axes. HRTEM images were obtained using a FEI TITAN 300 electron microscopy operating at 200 kV, also equipped with a double-tilt sample holder. All electron diffraction patterns were indexed using pseudo-cubic unit cell notations.

RESULTS AND DISCUSSION

Figures 1(a) and 1(b) show typical domain structures obtained by PFM for as-grown NBT and Mn-NBT. Randomly distributed polar nano-regions can be seen, as previously reported for NBT.[21,24] For as-grown NBT, the size of the polar regions ranged from 200 to 500 nm, with many regions of much smaller size randomly distributed there within. However, for as-grown Mn-NBT, the size of the polar regions was decreased to 100–200 nm and the domain distribution was more uniform. The smaller size of the polar regions for as-grown Mn-NBT may help explain a previously reported enhancement in the frequency dispersion of the dielectric constant in the temperature range of 373 K-473 K with Mn substitution.[49] When Mn-NBT was annealed at 970 K, the polar region size was found to coarsen, as shown in the PFM image given in Fig. 1(c). These results are different than the ones of NBT (Data of annealed NBT is not shown here. The size of domain size for NBT decreased to 100–300 nm.), where a domain refinement was found upon annealing. The differences on annealing between NBT and Mn-NBT in the PFM images indicate that Mn substitution reduced the polar domain size and resulted in good domain distribution, i.e., a more uniform domain distribution with a decreased size from 200–500 nm to 100–200 nm. These observed changes may originate from the Mn substitution and associated defect compensation, the details of which will be described in the proceeding section.

Based on these observed changes in size and distribution of polar regions, we can conclude that the degree of long-range polar ordering of NBT increases with Mn. We can quantify this observation by using a correlation function technique that has been applied to topography analysis,[56] where the signal contrast (D) taken from the piezoresponse

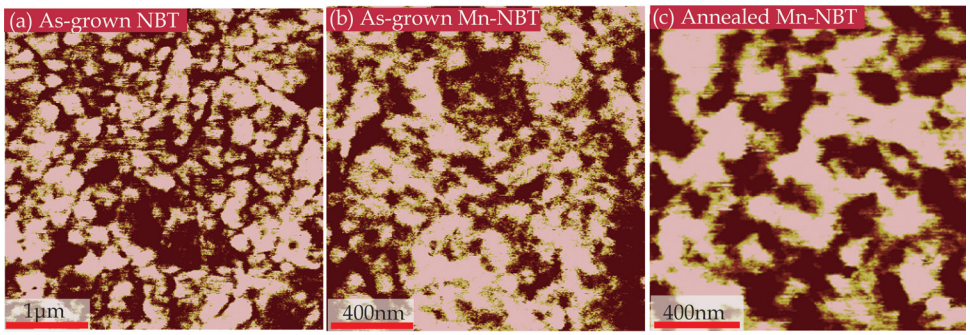

FIG. 1. Ferroelectric domain images of (a) as-grown NBT, (b) as-grown Mn-NBT, (c) annealed Mn-NBT.

image is then proportional to the local polarization. The autocorrelation function,

$$C(R_1, R_2) = \sum_{x,y} D(x, y)D(x + R_1, y + R_2), \qquad (1)$$

is equivalent to the polarization-polarization correlation function. It has been reported that the average correlation function can then be approximated as

$$C(R)\alpha \exp[(R/\xi)^{-2h}], \qquad (2)$$

where R is the radius, ξ is the correlation length, and h an exponent parameter.[56] It is believed that ξ is directly related to the average polar region size. Thus, it can serve as a measure of the polarization disorder (or quenched random fields).[53] The averaged autocorrelation function for the three PFM images is given in Fig. 2. It can be seen that the value of ξ increases from 36 nm for pure NBT to 41 nm for as-grown Mn-NBT, and, upon annealing Mn-NBT, ξ was further increased to 78 nm.

The valence of Mn is variable, but it is believed that the 3^+ valence of Mn in NBT is dominant.[57] Theoretically, Mn^{3+} can occupy either the B-site Ti^{4+} or an A-site vacancy. A-site occupancy is favored by considering the volatility of Bi^{3+} and Na^+. The ionic radius of Mn^{3+} is larger than that of Ti^{4+}, and the resistivity is increased by up to two orders of magnitude by Mn doping, implying that the occupancy of the A-site in NBT would be preferred, suppressing the concentration of oxygen vacancies.[4] Please note that the substitution of B-site Ti^{4+} by Mn^{3+} would induce oxygen vacancy formation, which could decrease the resistivity. When Mn is incorporated onto the A sites of NBT, the concentration of oxygen vacancy is decreased as $2Mn^{3+}2Bi^{3+} + 3O^{2-} \leftrightarrow 2Mn_{B1}^{X} + Bi_2O_3\uparrow$. Accordingly, conduction would be suppressed by Mn, which should enhance the high-temperature electrical resistivity. A-site occupancy of Mn is also supported by composition analysis previously reported by Nagata and Takenaka.[58]

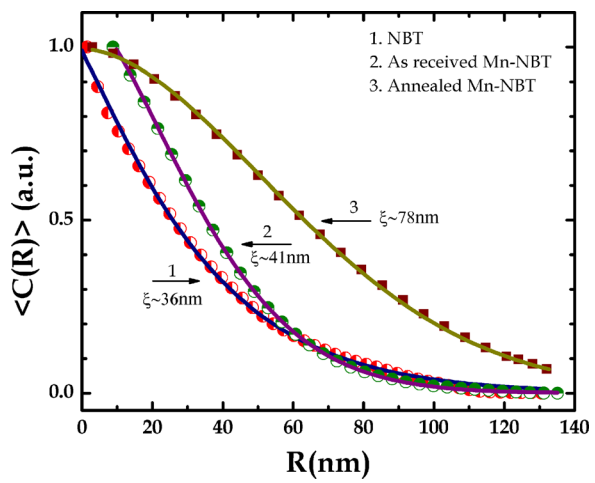

FIG. 2. The averaged autocorrelation function for as-grown NBT, as-grown Mn-NBT, and annealed Mn-doped NBT, respectively. The lines show the fit of experimental points to the equation $\langle C(R)\rangle \sim \exp\left[-\left(\frac{R}{\xi}\right)^{2h}\right]$.

Since O^{2-} is large and occupies the corner of the octahedron, ionic conduction via oxygen vacancies is relatively high at moderate temperatures. These crystal chemical considerations may help explain not only the changes in the dielectric loss factors and electrical resistance, but may also provide insights into the coarsening of the polar regions by Mn substitution and subsequent annealing. Mn substitution is known to impart "hard" characteristics to PZT and PMN-PT,[59,60] due to defect pinning. Based on the symmetry-conforming property of defects in ferroelectrics, one might anticipate higher degree of polar order in systems with defects that can pin the polarization,[61,62] rather than those of the random-field type.[63]

The size of the polar regions for NBT was prone to decrease upon annealing. (Data of annealed NBT is not shown here. The size of domain size for NBT decreased to 100–300 nm.) Oxygen vacancies may be randomly quenched-in on cooling from high temperature above the phase transformation. Random fields are known to disrupt the polar order,[62] favoring smaller polar domain sizes, as observed in the annealed NBT. In Mn-NBT, on one hand, the Mn doping probably prefers to suppress the random-field-type defects; on the other hand, a portion of the defects may be quenched-in on annealing that interacts strongly with domain boundaries on coolings, which pins the polarization. Then, annealing may result in the formation of extended defect structures along the domain boundaries, as previously reported for "hard" PZT.[56] This would result in large defect-free regions that allow for the achievement of larger-sized domain structures.

We then performed TEM and lattice imaging studies on Mn-NBT. These studies were done (i) to check whether the domains obtained by PFM reflected domain states, typical of the volume, as PFM only maps them out on the surface, and (ii) to obtain direct evidence of possible defects near the domain boundaries. First, we note that bright field images

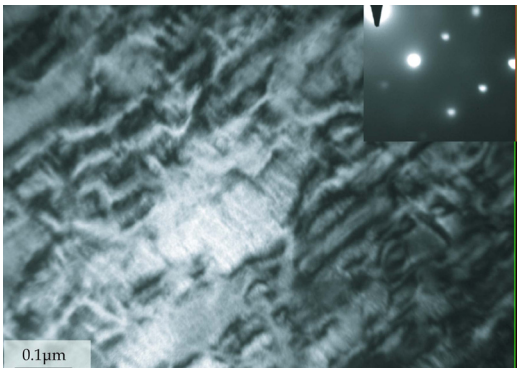

FIG. 3. Bright field TEM image, which shows nano-sized ferroelectric domains for Mn-NBT. The inset shows a SAED pattern taken along the [112] zone axis.

support the results by PFM. The bright field images revealed the presence of fine domain structures that were characterized by cross-hatched contrast, as shown in Fig. 3 for Mn-NBT. The features of this nanodomain structure are similar to that observed in the PFM image. Furthermore, the TEM images reveal that the polar regions of Mn-NBT were larger than those of NBT (data not shown).

Please note that, for our TEM/PFM studies, domain mapping was performed on several samples and over different regions of each sample. Comprehensive studies and analysis on two different compositions revealed that the patterns of pure NBT and Mn-NBT are different. The domain patterns shown in the manuscript are the typical ones, which represent those of the Mn-doped samples. Although Mn substitution is the major reason for the change of the domain, the effect of Na/Bi distribution still cannot be ignored.

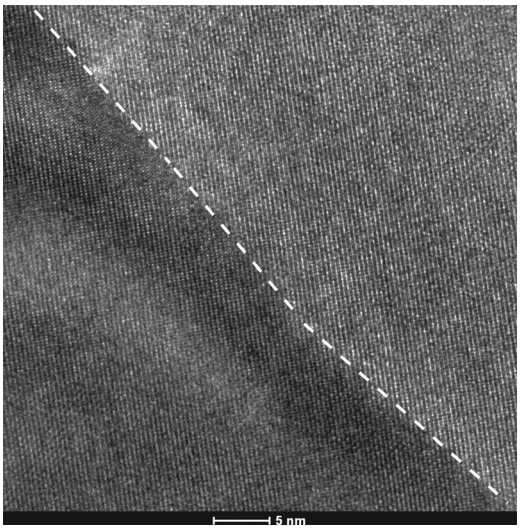

FIG. 4. High resolution electron micrograph of Mn-NBT along the [110] projection.

Next, lattice images were obtained for Mn-NBT near the nanodomain boundaries, as shown in Fig. 4. The boundary in this figure is marked by a dashed line. The image reveals that the lattice remains coherent across the boundary: few planar defects were found. This is in difference with recent studies of NBT,[34] where a large number of planar defects were found at the boundaries. For NBT, the elastic stress caused by the coexistence of T and R structures was believed to be partially

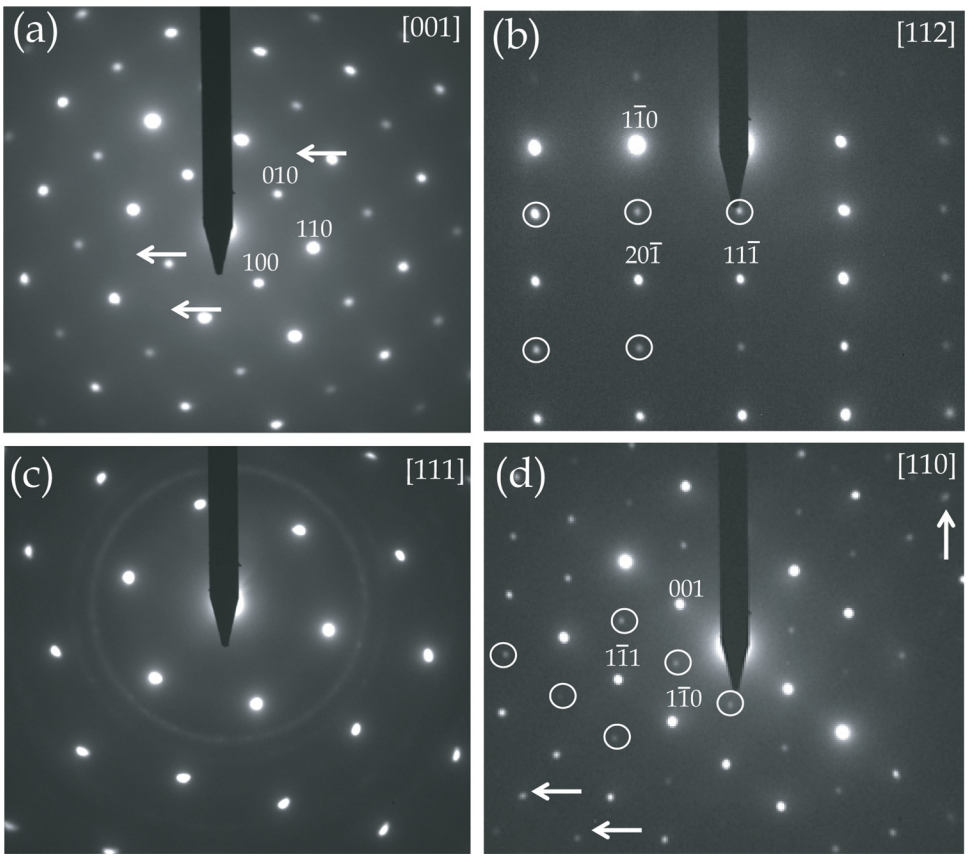

FIG. 5. (a)-(c) SAED patterns of Mn-NBT taken along the (a) [001], (b) [112], (c) [111], and (d) [110]. The arrows indicate the possible 1/2 (ooe) super-reflections from in-phase octahedral tilting, and the circles show the 1/2 (ooo) super-reflections from anti-phase octahedral tilting.

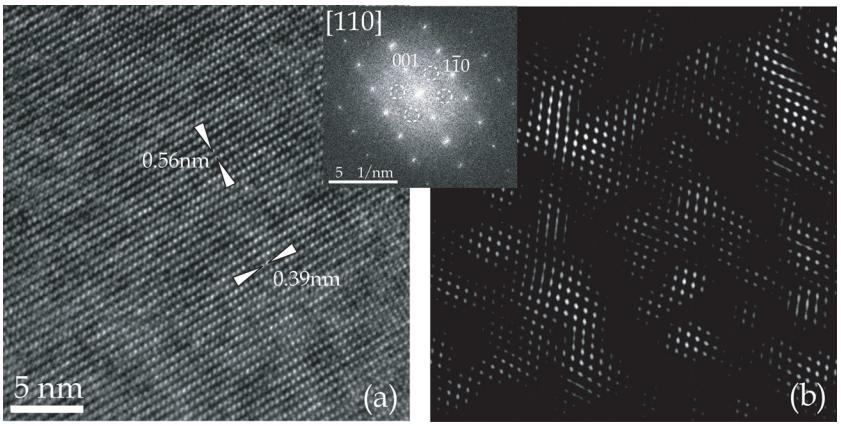

FIG. 6. (a) High resolution electron microscopy image of Mn-NBT along the [110] projection; (b) inverse Fourier transform of the super-reflections of image (a). The inset shows the power spectrum of the lattice image in (a), in which weak 1/2 (ooo) super-reflections were observed.

relaxed by lifting the lattice coherency across boundaries.[34] For Mn-NBT, there may be several reasons to explain the enhanced lattice coherency at the domain boundaries. First, the size of ferroelastic domains in Mn-NBT is decreased compared to NBT. High densities of small ferroelastic domains might more easily stress-accommodate each other. Second, Mn substitution at A sites would result in a decreased concentration of vacancies gathering at the boundaries to form planar defects that are required to lift coherency.

Figure 5 shows SAED patterns for Mn-NBT taken along the (a) [001], (b) [112], (c) [111], and (d) [110]. Weak 1/2 (ooe) reflections can be observed in Fig. 5(a), as marked by arrows, where o designates odd values of the Millers indices and e even. It has been noted that these superlattice reflections originate from slight deviations from the ideal perovskite structure, which could have intensity contributions from: (i) oxygen octahedral tilts; (ii) chemical ordering of the A-site cations; and/or (iii) antiparallel displacements of cations.[21,64–69] In NBT, following theoretical[21] and experimental studies,[68,69] it is believed that oxygen octahedral tilting is the dominate source of the intensity.[32,70]

Evidence of in-phase octahedral tilting in Mn-NBT at room temperature was apparent in (001) SAED patterns by weak 1/2 (ooe) superlattice reflections, as marked by an arrow in Fig. 5(a). This type of in-phase octahedral tilt system generally occurs in tetragonal structures,[64,69] whereas rhombohedral (R3c) structures of perovskite often have an anti-phase 1/2 (ooo) octahedral tilting about the pseudocubic axes.[64] In Figs. 5(b) and 5(d), 1/2 (ooo) reflections were found, as marked by circles. It is worth to note that 1/2 (ooe) reflections were also observed along [110], as marked by arrows in Fig. 5(d), indicating coexisting in-phase and anti-phase tiltings in Mn-NBT. However, no such 1/2 (ooe) reflections were apparent along [111] and [112]. The structure of NBT in the temperature range of 5–528 K has been reported to be a single-phase R, with an anti-phase 1/2 (ooo) octahedra tiling. However, in-phase 1/2 (ooe) octahedral tilts are known to become prominent between 528–800 K.[68] Dorcet and Trolliard[64] proposed, in this higher temperature range, that T and R phases coexist which have two different types of tilts (i.e., in-phase and anti-phase) that need to be accommodated. It should be noticed that, in the [011] zone axis pattern of their work, the expected 1/2 (ooe) extra spots of the T phase were not observed: this implies a systematic extinction, corresponding to a glide plane.

However, in the [011] zone axis pattern for Mn-NBT, the expected 1/2 (ooe) extra spots were indeed observed, as marked by arrows in Fig. 5(d). This indicates that glide planes in Mn-NBT are present and that tetragonal in-phase tilting has become more pronounced. This can also be explained by the Goldschmidt tolerance factor,[70]

$$t = \frac{R_A + R_O}{\sqrt{2}(R_B + R_O)},$$

where R_A, R_B, and R_O are ionic radii of A and B cations and oxygen in the ABO_3 perovskite structure, respectively. Compounds in the perovskite family are found to exist over the tolerance factor range $1.05 > t > 0.78$.[70] An in-phase tilting distortion generally has a smaller value of t than anti-phase ones. It is known that Mn substitution is incorporated onto the A sites and that the ionic radius of Mn^{3+} (0.65 Å) is significantly smaller than Bi^{3+} (1.28 Å) or Na^{+} (1.39 Å): this could decrease the value of t and, accordingly, suppress anti-phase rotations, producing slightly more intense 1/2 (ooe) reflections.

Due to the weak intensity of in-phase 1/2 (ooe) super-reflections in Mn-NBT, it was extremely difficult to study the 1/2 (ooe) one using HRTEM. Accordingly, only the octahedral anti-phase 1/2 (ooo) superlattice reflections were investigated. A lattice image for Mn-NBT taken along the [110] zone axis and the corresponding power spectrum are shown in Fig. 6(a). 1/2 (ooo) superlattice reflections were obvious in the power spectrum, as marked by dashed circles. In order to obtain more detailed information about the anti-phase tilts, inverse Fourier transforms of these super-reflections were obtained. The corresponding image is shown in Fig. 6(b). In this image, lattice clusters of size 3–8 nm can be seen. It can be inferred that the 1/2 (ooe) in-phase tilted domains for Mn-NBT would be of similar or smaller size, but notably lower density. The enhanced ferroelectric ordering and in-phase octahedral tilting may help explain the enhanced piezoelectric properties of NBT with Mn.[49]

CONCLUSION

The ferroelectric domain structures of pure NBT and 1 at.% Mn-doped NBT (Mn-NBT) single crystals were investigated by PFM. The correlation length of the polar clusters was found to increase from 36 nm (NBT) to 78 nm (Mn-NBT,

annealed). In addition, SAED revealed 1/2 (ooo) octahedral tiltings for NBT. Coexisting in-phase 1/2 (ooe) and anti-phase 1/2 (ooo) tiltings were found on Mn substitution.

ACKNOWLEDGMENTS

This work was financially supported by the National Science Foundation (Materials World Network) DMR-0806592, by the Department of Energy under DE-FG02-07ER46480, by the National Science Foundation of China 50602047, by the Shanghai Municipal Government 08JC1420500, and by the Programme of Creation and Development of the National University of Science and Technology (MISiS). J. Yao also would like to thank the financial support from the China Scholarship Council. Authors also give thanks to Dr. Z. K. Xu for useful discussion and NCFL in Virginia Tech for the TEM support.

[1]S. Park and T. R. Shrout, J. Appl. Phys. **82**, 1804 (1997).
[2]Y. Saito, H. Takao, T. Tani, T. Nonoyama, K. Takatori, T. Homma, T. Nagaya, and M. Nakamura, Nature **432**, 84 (2004).
[3]Y. M. Chiang, G. W. Farrey, and A. N. Soukhojak, Appl. Phys. Lett. **73**, 3683 (1998).
[4]Q. Zhang, Y. Zhang, F. Wang, Y. Wang, D. Lin, X. Zhao, H. Luo, W. Ge, and D. Viehland, Appl. Phys. Lett. **95**, 102904 (2009).
[5]J. J. Yao, Y. D. Yang, N. Monsegue, Y. X. Li, J. F. Li, Q. H. Zhang, W. W. Ge, H. S. Luo, and D. Viehland, Appl. Phys. Lett. **98**, 132903 (2011).
[6]F. Cordero, F. Craciun, F. Trequattrini, E. Mercadelli, and C. Galassi, Phys. Rev. B **81**, 144124 (2010).
[7]Y. P. Guo, M. Y. Gu, H. S. Luo, Y. Liu, and R. L. Withers, Phys. Rev. B **83**, 054118 (2011).
[8]J. Rodel, W. Jo, K. Seifert, E. M. Anton, T. Granzow, and D. Damjanovic, J. Am. Ceram. Soc. **92**, 1153 (2009).
[9]D. Rout, K.-S. Moon, V. S. Rao, and S.-J. Kang, J. Am. Ceram. Soc. **117**, 797 (2009).
[10]J. Kling, X. L. Tan, W. Jo, H.-J. Kleebe, H. Fuess, and J. Rödel, J. Am. Ceram. Soc. **93**, 2452 (2010).
[11]W. Jo, S. Schaab, E. Sapper, L. A. Schmitt, H.-J. Kleebe, A. J. Bell, and J. Rödel, J. Appl. Phys. **110**, 074106 (2011).
[12]W. Jo, J. Daniels, J. L. Jones, X. Tan, P. A. Thomas, D. Damjanovic, and J. Rodel, J. Appl. Phys. **109**, 014110 (2011).
[13]E. Sapper, S. Schaab, W. Jo, T. Granzow, and J. Rödel, J. Appl. Phys. **111**, 014105 (2012).
[14]S. Gorfman and P. A. Thomas, J. Appl. Crystallogr. **43**, 1409 (2010).
[15]S. B. Vakhrushev, V. A. Isupov, B. E. Kvyatkovsky, N. M. Okuneva, I. P. Pronin, G. A. Smolensky, and P. P. Syrnikov, Ferroelectrics **63**, 153 (1985).
[16]J. Suchanicz and J. Kapulinski, Ferroelectrics **165**, 249 (1995).
[17]I. G. Siny, C.-S. Tu, and V. H. Schmidt, Phys. Rev. B **51**, 5659 (1995).
[18]S. V. Vakhrushev, B. E. Kvyatkovsky, R. S. Malysheva, N. M. Okuneva, E. L. Plachenova, and P. P. Syrnikov, Sov. Phys. Crystallogr. **34**, 89 (1989).
[19]C.-S. Tu, I. G. Siny, and V. H. Schmidt, Phys. Rev. B **49**, 11550 (1994).
[20]J. Kusz, J. Suchanicz, H. Bohm, and J. Warczewski, Phase Transitions **70**, 223 (1999).
[21]G. Jones and P. Thomas, Acta Crystallogr. B **58**, 168 (2002); **56**, 426 (2000).
[22]J. J. Yao, W. W. Ge, L. Luo, J. F. Li, D. Viehland, and H. Luo, Appl. Phys. Lett. **96**, 222905 (2010).
[23]V. Dorcet, G. Trolliard, and P. Boullay, Chem. Mater. **20**, 5061 (2008).
[24]G. Trolliard and V. Dorcet, Chem. Mater. **20**, 5074 (2008).
[25]J. J. Yao, W. W. Ge, Y. D. Yang, L. Luo, J. F. Li, D. Viehland, S. Bhattacharyya, Q. H. Zhang, and H. S. Luo, J. Appl. Phys. **108**, 064114 (2010).
[26]B. Wylie-van Eerd, D. Damjanovic, N. Klein, N. Setter, and J. Trodahl, Phys. Rev. B **82**, 104112 (2010).
[27]C. Ma, X. Tan, E. Dul'kin, and M. Roth, J. Appl. Phys. **108**, 104105 (2010); C. Ma and X. Tan, Solid State Commun. **150**, 1497 (2010).
[28]B. Noheda, D. E. Cox, G. Shirane, J. A. Gonzalo, L. E. Cross, and S.-E. Park, Appl. Phys. Lett. **74**, 2059 (1999).
[29]R. Guo, L. E. Cross, S.-E. Park, B. Noheda, D. E. Cox, and G. Shirane, Phys. Rev. Lett. **84**, 5423 (2000).
[30]D. Viehland, J. Appl. Phys. **88**, 4794 (2000).
[31]B. Noheda, D. E. Cox, G. Shirane, J. Gao, and Z. G. Ye, Phys. Rev. B **66**, 054104 (2002).
[32]M. Davis, D. Damjanovic, and N. Setter, Phys. Rev. B **73**, 014115 (2006).
[33]H. Cao, C. Stock, G. Y. Xu, P. M. Gehring, J. F. Li, and D. Viehland, Phys. Rev. B **78**, 104103 (2008).
[34]J. J. Yao, H. Cao, W. W. Ge, J. F. Li, and D. Viehland, Appl. Phys. Lett. **95**, 052905 (2009).
[35]J. Peräntie, J. Hagberg, A. Uusimäki, and H. Jantunen, Phys. Rev. B **82**, 134119 (2010).
[36]Z. Xu, X. H. Dai, and D. Viehland, Phys. Rev. B **51**, 6261 (1995).
[37]Z. Xu, X. H. Dai, J. F. Li, and D. Viehland, Appl. Phys. Lett. **68**, 1628 (1996).
[38]Z. Xu, X. H. Dai, J. F. Li, and D. Viehland, Appl. Phys. Lett. **71**, 2280 (1997).
[39]Q. Tan, Z. Xu, J. F. Li, and D. Viehland, Appl. Phys. Lett. **71**, 1062 (1997).
[40]E. Garcia-Gonzalez, A. Torres-Pardo, R. Jimenez, and J. M. Gonzalez-Calbet, Chem. Mater. **19**, 3575 (2007).
[41]A. Torres-Pardo, R. Jimenez, J. M. Gonzalez-Calbet, and E. Garcia-Gonzalez, Chem. Mater. **20**, 6957 (2008).
[42]A. Torres-Pardo, R. Jimenez, J. M. Gonzalez-Calbet, and E. Garcia-Gonzalez, Chem. Mater. **21**, 2193 (2009).
[43]A. Torres-Pardo, R. Jimenez, J. M. Gonzalez-Calbet, and E. Garcia-Gonzalez, J. Am. Chem. Soc. **132**, 9843 (2010).
[44]C. J. Cheng, D. Kan, S. H. Lim, W. R. McKenzie, P. R. Munroe, L. G. Salamanca-Riba, R. L. Withers, I. Takeuchi, and V. Nagarajan, Phys. Rev. B **80**, 014109 (2009).
[45]S. Karimi, I. M. Reaney, I. Levin, and I. Sterianou, Appl. Phys. Lett. **94**, 112903 (2009).
[46]C. H. Yang, J. Seidel, S. Y. Kim, P. B. Rossen, P. Yu, M. Gajek, Y. H. Chu, L. W. Martin, M. B. Holcomb, Q. He, P. Maksymovych, N. Balke, S. V. Kalinin, A. P. Baddorf, S. R. Basu, M. L. Scullin, and R. Ramesh, Nature Mater. **8**, 485 (2009).
[47]J. Schiemer, R. Withers, L. Noren, Y. Liu, L. Bourgeois, and G. Stewart, Chem. Mater. **21**, 4223 (2009).
[48]D. Kan, L. Palova, V. Anbusathaiah, C. J. Cheng, S. Fujino, V. Nagarajan, K. M. Rabe, and I. Takeuchi, Adv. Funct. Mater. **20**, 2436 (2010).
[49]W. W. Ge, J. F. Li, D. Viehland, and H. Luo, J. Am. Ceram. Soc. **93**, 1372 (2010).
[50]E. Aksel, H. Foronda, K. Calhoun, J. L. Jones, S. Schaab, and T. Granzow, Funct. Mater. Lett. **3**, 45 (2010).
[51]C.-S. Tu, S.-H. Huang, C.-S. Ku, H.-Y. Lee, R. R. Chien, H. Schmidt, and H. Luo, Appl. Phys. Lett. **96**, 062903 (2010).
[52]N. Balke, I. Bdikin, S. V. Kalinin, and A. L. Kholkin, J. Am. Ceram. Soc. **92**, 1629 (2009).
[53]D. A. Kiselev, I. K. Bdikin, E. K. Selezneva, K. Bormanis, A. Sternberg, and A. L. Kholkin, J. Appl. D: Appl. Phys. **40**, 7109 (2007).
[54]A. Yourdkhani, A. K. Perez, C. Lin, and G. Caruntu, Chem. Mater. **22**, 6075 (2010).
[55]J. J. Yao, L. Yan, W. W. Ge, L. Luo, J. F. Li, D. Viehland, Q. H. Zhang, and H. Luo, Phys. Rev. B **83**, 054107 (2011).
[56]R. C. Munoz, G. Vidal, M. Mulsow, J. G. Lisoni, C. Arenas, and A. Concha, Phys. Rev. B **62**, 4686 (2000).
[57]Y. S. Sung and M. H. Kim, *Ferroelectrics*, edited by I. Coondoo (InTech, 2010).
[58]H. Nagata and T. Takenaka, J. Eur. Ceram. Soc. **21**, 1299 (2001).
[59]Y. K. Gao, K. Uchino, and D. Viehland, Jpn. J. Appl. Phys. **45**, 9119 (2006).
[60]S. J. Zhang, S. M. Lee, D. H. Kim, H. Y. Lee, and T. R. Shrout, Appl. Phys. Lett. **93**, 122908 (2008).
[61]X. Ren, Nature Mater. **3**, 91 (2004).
[62]L. X. Zhang and X. Ren, Phys. Rev. B **71**, 174109 (2005); **73**, 094121 (2006).
[63]D. Viehland, X. H. Dai, J. F. Li, and Z. K. Xu, J. Appl. Phys. **84**, 458 (1998).
[64]V. Dorcet and G. Trolliard, Acta Mater. **56**, 1753 (2008).
[65]A. Soukhojak, H. Wang, G. Farrey ,and Y.-M. Chang, J. Phys. Chem. Solids **61**, 301 (2000).
[66]C. W. Tai and Y. Leraah, Appl. Phys. Lett. **95,** 062801 (2009).
[67]V. Dorcet, G. Trolliard, and P. Boullay, J. Magn. Magn. Mater. **321**, 1758 (2009).
[68]P. M. Woodward, Acta Crystallogr. B **53**, 44 (1997).
[69]D. I. Woodward and I. M. Reaney, Acta Crystallogr. B **61**, 387 (2005).
[70]I. M. Reaney, E. L. Colla, and N. Setter, Jpn. J. Appl. Phys. **33**, 3984 (1994).